J. Fluid Mech. (1995), *vol.* 283, *pp.* 329–340

Nonlinear Taylor–Couette flow of helium II

By KAREN L. HENDERSON[1], CARLO F. BARENGHI[1] AND CHRIS A. JONES[2]

[1] Department of Mathematics, University of Newcastle, Newcastle upon Tyne, NE1 7RU, UK

[2] Department of Mathematics, University of Exeter, Exeter, EX4 4QE, UK

(Received 24 December 1993 and in revised form 25 August 1994)

We solve the nonlinear two-fluid Hall–Vinen–Bekharevich–Khalatnikov equations of motion of helium II for the first time and investigate the configuration of quantized vortex lines in Taylor–Couette flow. The results are interpreted in terms of quantities which can be observed by measuring the attenuation of second sound. Comparison is made with existing experimental results.

1. Introduction

Vortex line configurations have always attracted much attention and have been studied in a variety of superfluid systems (Donnelly 1991), ranging from simple equilibrium flows, such as rotating cylinders (Hall & Vinen 1956) or annuli (Bendt 1967), to complicated turbulent pipe flows (Tough 1982; Donnelly & Swanson 1986). In the former systems, the methods of thermodynamics have been applied to determine the spatial structure of the vortices (Campbell & Ziff 1978). In the latter systems, computer simulations based on the laws of vortex dynamics (Schwarz 1988) have shed light on the problem of the superfluid vortex tangle. It is the case of simple but non-equilibrium flows, like the flow between two rotating concentric cylinders (Donnelly & Lamar 1988) Taylor–Couette flow), which is our concern here. In fluid mechanics the study of Taylor–Couette flow has led to many advances, from G. I. Taylor's successful application of linear stability theory, which established a firm ground for the use of the Navier–Stokes equations and the no-slip boundary conditions, to more recent understanding of transitions and nonlinear behaviour (Di Prima & Swinney 1981).

The most generally accepted equations for the macroscopic motion of helium II are the Hall–Vinen–Bekharevich–Khalatnikov equations (Hall 1960; Hall & Vinen 1954; Bekharevich & Khalatnikov 1961; Khalatnikov 1965), hereinafter referred to as the HVBK equations. The HVBK equations, derived in final form by Hills and Roberts (1977), generalize Landau's two-fluid model to take into account the presence of quantized vorticity. Although these equations have been tested experimentally, in general these tests have hitherto only been of linear perturbations around simple basic states. There is also some doubt as to the most appropriate boundary conditions which should be used with the HVBK equations (Hills & Roberts 1977).

Despite the early pioneering attempts of Chandrasekhar & Donnelly (1957) and the work of Snyder (1974) to use the HVBK equations to study the superfluid Taylor–Couette problem, contact between theory and experiments is very recent. Swanson & Donnelly's measurements (1991) of the speed of rotation of the inner cylinder at which toroidal motion begins have confirmed the predictions of Barenghi & Jones (1988) and Barenghi (1992) based on the HVBK theory. What Barenghi and Jones have calculated is the temperature dependent critical velocity Ω_{1c} at which the Couette azimuthal motion becomes unstable to infinitesimal axisymmetric per-

turbations of axial wavenumber k_c. Further support of the theory results from the more recent works of Bielert (1993) and of Barenghi, Swanson & Donnelly (1994) in the case of counter-rotating cylinders. The success of the linear stability theory has opened the way to study the development of the flow above onset. The aim of this paper is to present the first investigation of nonlinear superfluid Taylor–Couette flow. The question which we address is very simple: what is the configuration of the vortex lines above Ω_{1c}? Are the vortices still predominantly in the axial direction, as they are before the onset of instability, or are they churned into vortex-ring structures, with a large, predominantly azimuthal vorticity?

To appreciate why, until now, this simple question was still without an answer, one should consider the problem of flow visualization. In the classical Taylor–Couette case the flow pattern is no mystery. The introduction of flakes or other small particles in the working fluid (usually water or oil) is enough to make the Taylor cells visible to the eye. In the helium case, flow visualization at temperatures around two degrees above absolute zero is much harder. Recently, attempts have been made (Bielert 1993) to reveal the flow pattern by the addition of small particles. It is also possible to detect the position and the orientation of the quantized vortex lines. This is done by using a form of wave motion in superfluid helium, second sound, which directly probes the vorticity. In principle, simultaneous measurements of the attenuation of second sound along the axial, azimuthal and radial directions between the cylinders should disclose the vortex pattern and answer the question which we have addressed. In practice the information obtained is less complete than this, but hopefully the theory can guide the experimentalists and suggest exactly which measurements need be done.

While solving this problem, we seek at the same time a full validation of the nonlinear HVBK equations and their boundary conditions. The importance of the HVBK equations is that they are the fundamental equations of two-fluid hydrodynamics in the most general, rotational case.

Confidence in the HVBK equations should lead to their use in the study of helium flow problems which are still unsolved. For example, the computer simulations of the vortex tangle give vortex configurations which depend, even at small Reynolds numbers just above onset, on the assumed normal fluid velocity profile in the channel (Aarts & de Waele 1994). The HVBK equations, on the contrary, determine the normal fluid velocity in a consistent way.

2. The model

We use cylindrical coordinates (r, ϕ, z) and consider superfluid helium at temperature T contained between two concentric cylinders of inner radius R_1 and outer radius R_2. The outer cylinder is held fixed and the inner cylinder rotates at constant angular velocity Ω_1. We make the usual simplifying assumption (Chandrasekhar 1961) that the cylinders have infinite length; this is valid only if the temperature is in the region just below T_λ, where the critical wavelength is still comparable with the size of the gap (Barenghi & Jones 1988; Barenghi 1992). The incompressible HVBK equations, which describe a macroscopic fluid containing many vortex lines, are

$$\frac{\partial \boldsymbol{v}^n}{\partial t} + (\boldsymbol{v}^n \cdot \boldsymbol{\nabla})\, \boldsymbol{v}^n = -\boldsymbol{\nabla} p^n + \nu^n \boldsymbol{\nabla}^2 \boldsymbol{v}^n + \frac{\rho^s}{\rho} \boldsymbol{F}, \tag{1}$$

$$\frac{\partial \boldsymbol{v}^s}{\partial t} + (\boldsymbol{v}^s \cdot \boldsymbol{\nabla})\, \boldsymbol{v}^s = -\boldsymbol{\nabla} p^s - \nu^s \boldsymbol{T} - \frac{\rho^n}{\rho} \boldsymbol{F}, \tag{2}$$

$$\boldsymbol{\nabla} \cdot \boldsymbol{v}^n = 0, \quad \boldsymbol{\nabla} \cdot \boldsymbol{v}^s = 0, \tag{3}$$

where $\boldsymbol{v}^n$ and $\boldsymbol{v}^s$ are the normal fluid and superfluid velocities, ρ^n and ρ^s are the normal fluid and superfluid densities, $\rho = \rho^n + \rho^s$ is the total density of helium, $\boldsymbol{\omega}^s = \boldsymbol{\nabla} \times \boldsymbol{v}^s$ is the superfluid vorticity, $\hat{\boldsymbol{\omega}}^s = \boldsymbol{\omega}^s/|\boldsymbol{\omega}^s|$, p^n and p^s are effective pressures, $\nu^n = \mu/\rho^n$ is the normal fluid kinematic viscosity, μ is the helium viscosity, $\nu^s = (\Gamma/4\pi)\log(b_0/a_0)$ is the vortex tension parameter where a_0 is the vortex core radius, b_0 is the intervortex spacing and Γ is the quantum of circulation. The mutual friction force (Barenghi, Donnelly & Vinen 1983) is

$$\boldsymbol{F} = \tfrac{1}{2}B\hat{\boldsymbol{\omega}}^s \times (\boldsymbol{\omega}^s \times (\boldsymbol{v}^n - \boldsymbol{v}^s - \nu^s \boldsymbol{\nabla} \times \hat{\boldsymbol{\omega}}^s)) + \tfrac{1}{2}B'\boldsymbol{\omega}^s \times (\boldsymbol{v}^n - \boldsymbol{v}^s - \nu^s \boldsymbol{\nabla} \times \hat{\boldsymbol{\omega}}^s)), \tag{4}$$

where B and B' are the mutual friction coefficients, and the vortex tension force $-\nu^s \boldsymbol{T}$ is given by

$$\boldsymbol{T} = \boldsymbol{\omega}^s \times (\boldsymbol{\nabla} \times \hat{\boldsymbol{\omega}}^s). \tag{5}$$

A solution of the HVBK equations which is stable at low rotation rate is the Couette velocity profile $\boldsymbol{v}^n = \boldsymbol{v}^s = \boldsymbol{v}^0 = (ar + b/r)\,\hat{\boldsymbol{e}}_\phi$, where $\hat{\boldsymbol{e}}_\phi$ is the unit vector in the azimuthal direction and the parameters $a = -\Omega_1 R_1^2/(R_2^2 - R_1^2)$ and $b = \Omega_1 R_1^2 R_2^2/(R_2^2 - R_1^2)$ are chosen to satisfy the boundary conditions $v_\phi^0(r = R_1) = \Omega_1 R_1$ and $v_\phi^0(r = R_2) = 0$. This Couette state corresponds to vortex lines of uniform density

$$n^0 = 2|a|/\Gamma, \tag{6}$$

aligned along the axis of rotation. It is convenient to make the equations dimensionless by introducing a lengthscale based on the gap width $\delta = R_2 - R_1$ and a timescale δ^2/ν^n based on the normal fluid diffusion. The solution of the HVBK equations is then determined by the radius ratio $\eta = R_1/R_2$ and the Reynolds number $Re_1 = \Omega_1 R_1 \delta/\nu^n$.

To investigate the nonlinear solution above onset we write the total velocity fields as $\boldsymbol{v}_{tot}^n = \boldsymbol{v}^n + \boldsymbol{v}^0$ and $\boldsymbol{v}_{tot}^s = \boldsymbol{v}^s + \boldsymbol{v}^0$. It is convenient to introduce the stream functions ψ^n and ψ^s

$$\boldsymbol{v}^n = \left(-\frac{1}{r}\frac{\partial \psi^n}{\partial z}, v_\phi^n, \frac{1}{r}\frac{\partial \psi^n}{\partial r}\right); \quad \boldsymbol{v}^s = \left(-\frac{1}{r}\frac{\partial \psi^s}{\partial z}, v_\phi^s, \frac{1}{r}\frac{\partial \psi^s}{\partial r}\right), \tag{7}$$

for which equations (3) are automatically satisfied. We solve the equations for the azimuthal velocity components v_ϕ^n and v_ϕ^s and for the potential vorticities $Z^n = \omega_\phi^n/r = (\boldsymbol{\nabla} \times \boldsymbol{v}^n)_\phi/r$ and $Z^s = \omega_\phi^s/r = (\boldsymbol{\nabla} \times \boldsymbol{v}^s)_\phi/r$, obtained by taking the curl of (1) and (2). These equations have the form

$$\frac{\partial Z^n}{\partial t} = L_1 Z^n + N_1, \quad \frac{\partial v_\phi^n}{\partial t} = L_2 v_\phi^n + N_2, \tag{8}$$

$$\frac{\partial Z^s}{\partial t} = N_3, \quad \frac{\partial v_\phi^s}{\partial t} = N_4, \tag{9}$$

and must be accompanied by the relations between stream functions and vorticities

$$Z^n + L_3 \psi^n = 0, \quad Z^s + L_3 \psi^s = 0. \tag{10}$$

L_1, L_2 and L_3 are linear operators defined by

$$L_1 = \frac{\partial^2}{\partial x^2} + \frac{3}{r}\frac{\partial}{\partial x} + \frac{\partial^2}{\partial z^2}, \tag{11}$$

$$L_2 = \frac{\partial^2}{\partial x^2} + \frac{1}{r}\frac{\partial}{\partial x} - \frac{1}{r^2} + \frac{\partial^2}{\partial z^2}, \tag{12}$$

$$L_3 = \frac{1}{r^2}\frac{\partial^2}{\partial x^2} - \frac{1}{r^3}\frac{\partial}{\partial x} + \frac{1}{r^2}\frac{\partial^2}{\partial z^2}, \tag{13}$$

where $x = r - \eta/(1-\eta)$, and N_1, N_2, N_3 and N_4 are the nonlinear quantities:

$$N_1 = \frac{2}{r^2}(v_\phi^0 + v_\phi^n)\frac{\partial v_\phi^n}{\partial z} + \frac{1}{r}\frac{\partial(\psi^n, Z^n)}{\partial(z,x)} + \frac{\rho^s}{\rho r}\left(\frac{\partial F_r}{\partial z} - \frac{\partial F_z}{\partial x}\right), \tag{14}$$

$$N_2 = \frac{1}{r}\left(2a + \frac{v_\phi^n}{r}\right)\frac{\partial \psi^n}{\partial z} + \frac{1}{r}\frac{\partial(\psi^n, v_\phi^n)}{\partial(z,x)} + \frac{\rho^s}{\rho}F_\phi, \tag{15}$$

$$N_3 = \frac{2}{r^2}(v_\phi^0 + v_\phi^s)\frac{\partial v_\phi^s}{\partial z} + \frac{1}{r}\frac{\partial(\psi^s, Z^s)}{\partial(z,x)} + \frac{\rho^n}{\rho r}\left(\frac{\partial F_r}{\partial z} - \frac{\partial F_z}{\partial x}\right) - \frac{\beta}{r}\left(\frac{\partial T_r}{\partial z} - \frac{\partial T_z}{\partial x}\right), \tag{16}$$

$$N_4 = \frac{1}{r}\left(2a + \frac{v_\phi^s}{r}\right)\frac{\partial \psi^s}{\partial z} + \frac{1}{r}\frac{\partial(\psi^s, v_\phi^s)}{\partial(z,x)} + \frac{\rho^n}{\rho}F_\phi - \beta T_\phi, \tag{17}$$

where

$$\frac{\partial(f,g)}{\partial(x,y)} = \frac{\partial f}{\partial x}\frac{\partial g}{\partial y} - \frac{\partial f}{\partial y}\frac{\partial g}{\partial x},$$

and $\beta = \nu^s/\nu^n$.

To solve equations (8) and (9) we need boundary conditions. These conditions are not determined by the HVBK equations themselves; ultimately the correct boundary conditions are a matter to be decided by experiments, and there is at present no universal agreement about what these conditions should be. It is conceivable that the appropriate boundary conditions may vary in different experimental situations, e.g. different temperature regimes. One of the aims of this work is to investigate which boundary conditions give results in best agreement with Taylor–Couette experiments.

The normal fluid is viscous and satisfies no-slip boundary conditions $\boldsymbol{v}^n = 0$ at the walls, which imply

$$v_\phi^n = \psi^n = \frac{\partial \psi^n}{\partial r} = 0 \quad \text{at} \quad r = R_1 \text{ and } R_2. \tag{18}$$

Equation (18) determines the solution of the normal fluid equations, which are of sixth order. In distinction to the normal fluid, the superfluid is inviscid; a first condition for $\boldsymbol{v}^s$ is that there is no flow across the boundaries;

$$v_r^s = 0 \quad \text{at} \quad r = R_1 \text{ and } R_2. \tag{19}$$

However these relations, which are satisfied by the choice

$$\psi^s = 0 \quad \text{at} \quad r = R_1 \text{ and } R_2, \tag{20}$$

are not enough to determine the solution of the superfluid problem. In fact, when the vertical friction and vortex tension terms are included the superfluid problem is of sixth order, so that three equations are required at each boundary. Equation (20) supplies one equation so two further equations are required. The further boundary conditions we apply on the curved walls are

$$\omega_\phi^s = 0 \quad \text{at} \quad r = R_1 \text{ and } R_2, \tag{21}$$

$$v_\phi^s = 0 \quad \text{at} \quad r = R_1 \text{ and } R_2. \tag{22}$$

Note that (22) implies that the angular velocity of the superfluid is the same as that of the cylinders at $r = R_1$ and R_2. These conditions have a number of advantages. Equations (22) and (20) imply that the superfluid velocity at the walls is only in the axial direction. Equations (21) and (22), which is equivalent to $\omega_r^s = 0$, imply that the vorticity is also purely axial at the walls. In consequence, the velocity and the vorticity

at the walls are parallel, so there is no mutual friction at the boundaries. Since the vorticity is purely axial at the walls these boundary conditions are consistent with the Couette state, in which all the superfluid vorticity is in the axial direction up to the wall.

Our numerical experience suggests that this lack of mutual friction at the boundaries is very advantageous. Indeed, other boundary conditions which we have tried to impose, which have (often large) mutual friction near the walls, have led to codes which failed to converge.

Various other boundary conditions have been proposed in a number of different contexts (Hills & Roberts 1977; Andronikashvili & Mamaladze 1966). There is a 'smooth boundary' condition in which the superfluid vortices can slip freely on the surface, so that vortices terminate normal to the wall, giving

$$\boldsymbol{\omega}^s \times \hat{\boldsymbol{n}} = 0 \tag{23}$$

where $\hat{\boldsymbol{n}}$ is the unit vector normal to the wall. Taylor–Couette solutions using this boundary condition had large mutual friction at the boundary, which led to numerical instability. Possibly, adopting (23) leads to a boundary-layer structure which we were unable to resolve.

'Rough boundary' conditions in which the superfluid vortices are pinned to the curved walls are also conceivable. This suffers (possibly more severely) from the same problems as the smoth condition: a large mutual friction force developing at the boundary which cannot be handled numerically. Boundary conditions corresponding to partial slipping have also been discussed. Their drawback is that they require the knowledge of the slipping parameters.

We have integrated equations (8)–(10) together with boundary conditions (18)–(22) numerically, and have found well-converged solutions tending towards a nonlinear steady state with a number of different numerical schemes.

A difficulty, however, arises in using the boundary conditions (18)–(22) to solve the linear problem. The problem is that the terms containing the high-order radial derivatives disappear during the linearization process. In consequence, the linear problem is only second order in r, not sixth order. This second-order problem only requires one boundary condition at the curved walls, which is of course (20), and was the one solved satisfactorily by Barenghi & Jones (1988) and Barenghi (1992). The values of ω_ϕ^s and v_ϕ^s are then determined by the differential equations and cannot be assigned arbitrarily. How then are we to apply (21) and (22)? The numerical values of ω_ϕ^s and v_ϕ^s at the boundaries emerging from the linear solutions are small but non-zero. The solution to this difficulty must lie in the formation of a nonlinear boundary layer, whose lengthscale is dependent on the amplitude of the solution. The nonlinear terms involving the large radial derivatives should be restored; if the boundary-layer thickness scales with a negative power of the amplitude, this boundary layer will serve to being the values of ω_ϕ^s and v_ϕ^s down from their 'mainstream' value to zero at the boundary. We have not computed this nonlinear boundary layer in detail. We surmise that it cannot greatly affect the mainstream solution, since the form of our nonlinear numerical solutions 5% above critical are not very different from the form of our linear solutions. Physically, the significance of this nonlinear boundary layer is that it forms the region in which the vortex lines are made purely axial at the boundary.

One can ask what is the evidence for the Couette flow as the basic state from an experimental point of view. The answer is that at small angular velocities the attenuation of second sound is found to be proportional to Ω_1 (Swanson & Donnelly 1991), which is in agreement with (6). Moreover, as pointed out by Barenghi & Jones (1988), an alternative basic state solution of the HVBK equations is $\boldsymbol{v}^n = \boldsymbol{v}^0$ and $\boldsymbol{v}^s =$

$(c/r)\,\boldsymbol{e}_\phi$ where c is a constant. This solution, in which the superfluid is in potential flow, would correspond to a radial temperature gradient which has not been detected. In conclusion, the assumption that at small rotations the flow is in the Couette state $\boldsymbol{v}^n = \boldsymbol{v}^s = \boldsymbol{v}^0$ is consistent with the observations.

However good an approximation, the Couette state cannot be an exact solution for a number of reasons. First, the ends of the cylinders generate a weak circulation which makes the bifurcation at $\Omega_1 = \Omega_{1c}$ imperfect; this feature is also present in the classical Taylor–Couette problem. Secondly, experiments show the existence of a missing row of vortices near the walls (Northby & Donnelly 1970). This effect cannot be properly taken into account by the HVBK equations, which describe only the average superfluid velocity field over a region containing many vortex lines.

In conclusion the simplified model which we adopt consists of equations (8)–(10) together with the boundary conditions (18)–(22). The solution is found by time-stepping from an arbitrary initial condition until a steady state is reached. We use a pseudospectral method based on expansions over Chebyshev polynomials in the radial direction and trigonometric functions in the axial one (Barenghi 1991; Jones 1985). The details of the methods will be published elsewhere. Here it suffices to say that the solution is tested for spectral convergence: typically we use 10 Chebyshev polynomials and 6 trigonometric functions. We checked that the solution obtained by time-stepping, decays or grows in time if the Reynolds number is below or above the critical value known from our previous study of the linearized HVBK equations (Barenghi & Jones 1988; Barenghi 1992). Another important check consists of setting the mutual friction coefficients B and B' equal to zero, which reduces the normal fluid equation (1) to the Navier–Stokes equation. This allows us to compute classical nonlinear Taylor–Couette flow and to check our results against published values (Barenghi 1991; Jones 1985).

3. The results

The results of the calculation of nonlinear superfluid Taylor–Couette flow are presented in figures 1–5 which show contour plots of various quantities. Each figure extends over one period in the axial direction; the inner boundary $r = R_1$ and the outer boundary $r = R_2$ are on the left and right, respectively. The calculation is done for radius ratio $\eta = 0.976$, temperature $T = 2.1$ K and Reynolds number $Re_1 = 391$; this value of the driving parameter is just above (5.4%) the onset of toroidal motion at $Re_{1c} = 371$ and $k_c = 1.5$. Figures 1(*a*)–(*f*) show, respectively, the normal fluid stream function ψ^n, the potential vorticity Z^n, the azimuthal velocity v_ϕ^n, the total azimuthal velocity $v_\phi^n + v_\phi^0$, the radial velocity v_r^n and the axial velocity v_z^n. Figure 2 shows the same quantities calculated for the superfluid. These can be compared with classical Taylor–Couette flow (Barenghi 1991; Jones 1985); the normal fluid flow is quite similar to the classical flow, although the asymmetry between the rapid outflow jet and the slower inflow jet is more marked than in classical Taylor–Couette flow at this radius ratio. The superfluid flow is radically different from the classical flow, with additional weak counter-rotating eddies visible in figure 2(*a*). These are probably due to the influence of the vortex tension. The intensity of the mutual friction force in the azimuthal direction, F_ϕ, is shown in figure 3(*a*), whilst figure 3(*b*) shows the quantity $(\nabla \times \boldsymbol{F})_\phi$ which forces the vorticities. Similarly, figures 3(*c*) and 3(*d*) show the vortex tension terms $-\beta T_\phi$ and $-\beta(\nabla \times \boldsymbol{T})_\phi$.

We are now ready to answer the question which we have addressed concerning the spatial configuration of the vortex lines. The superfluid vorticity field contains the

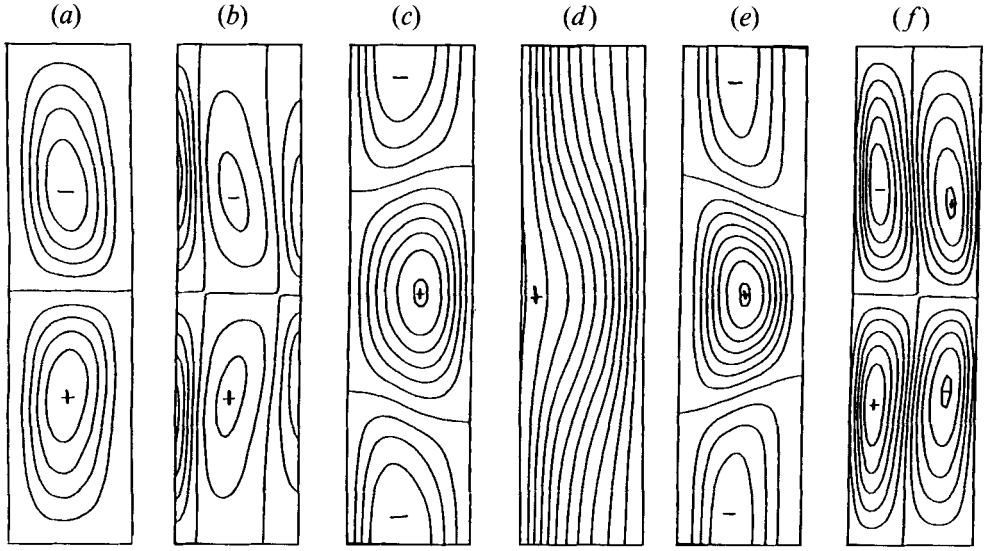

FIGURE 1. Normal fluid: (*a*) stream function ψ^n; (*b*) potential vorticity Z^n; (*c*) azimuthal velocity v_ϕ^n; (*d*) total azimuthal velocity $v_\phi^0+v_\phi^n$; (*e*) radial velocity v_r^n; (*f*) axial velocity v_z^n.

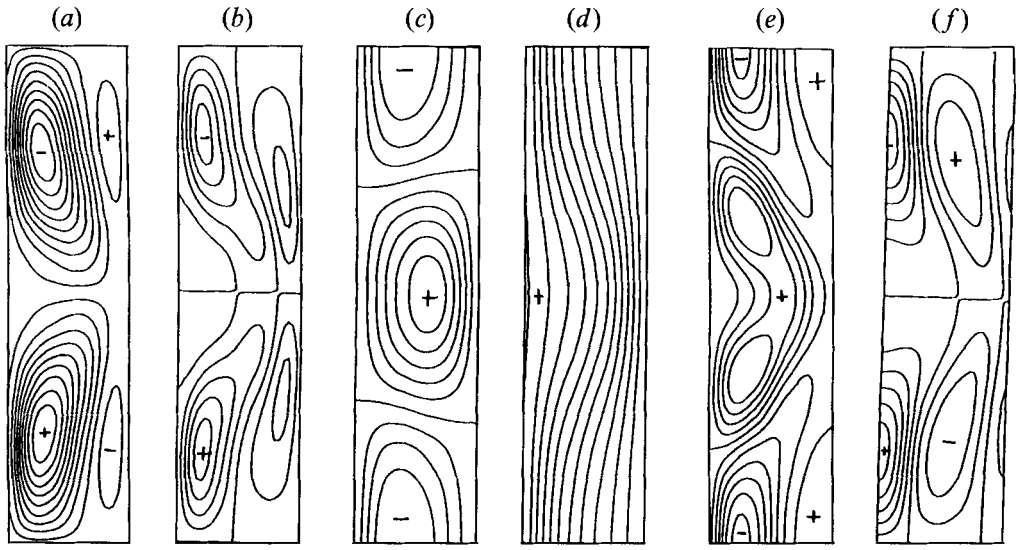

FIGURE 2. Superfluid: (*a*) stream function ψ^s; (*b*) potential vorticity Z^s; (*c*) azimuthal velocity v_ϕ^s; (*d*) total azimuthal velocity $v_\phi^0+v_\phi^s$; (*e*) radial velocity v_r^s; (*f*) axial velocity v_z^s.

information which we need, because the local density of vortex lines in the direction of a unit vector $\boldsymbol{p}$ is given by $(\boldsymbol{\omega}_{tot}^s\cdot\boldsymbol{p})/\Gamma$. Figure 4 shows the three components of the total vorticity of the superfluid. The peak values are approximately $|\omega_{r,tot}^s|\simeq 120$, $|\omega_{z,tot}^s|\simeq 690$ and $|\omega_{\phi,tot}^s|\simeq 19$. It is also interesting to compute mean values, averaged over a Taylor cell of length $2\pi/k$. Given any quantity $f=f(r,z)$ we define its mean value as

$$\langle f\rangle=\int_0^{2\pi/k}\mathrm{d}z\int_{R_1}^{R_2}rf(r,z)\,\mathrm{d}r\Big/\left(\int_0^{2\pi/k}\mathrm{d}z\int_{R_1}^{R_2}r\,\mathrm{d}r\right). \tag{24}$$

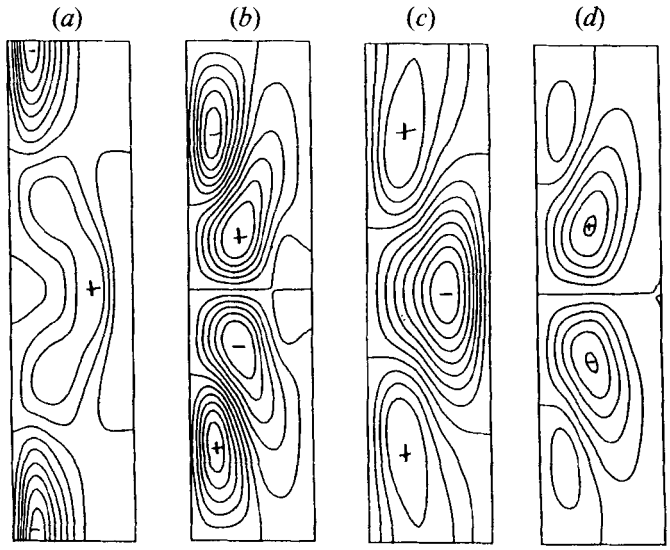

FIGURE 3. Mutual friction force and vortex tension force: (a) F_ϕ; (b) $(\nabla \times F)_\phi$; (c) $-\beta T_\phi$; (d) $-\beta(\nabla \times T)_\phi$.

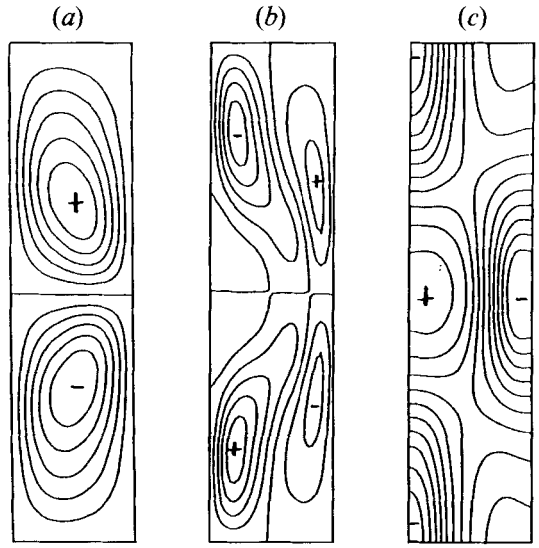

FIGURE 4. Total superfluid vorticity: (a) $\omega^s_{r,tot}$; (b) $\omega^s_{\phi,tot}$; (c) $\omega^s_{z,tot}$.

We find $\langle|\omega^s_{r,tot}|\rangle = 44.64$, $\langle|\omega^s_{z,tot}|\rangle = 386.25$ and $\langle|\omega^s_{\phi,tot}|\rangle = 5.02$. If we compare these numbers with the total amount of vorticity $2|a| = 386.25$ in the Couette state, in which the vortex lines are aligned along the axis or rotation, we conclude that the vortices are still predominantly in the z-direction and that the deflection along ϕ is small. Figure 5 shows explicitly the direction fields of the vortex lines in the (r, z)-plane at Reynolds numbers of $Re_{1c} = 371$ and $Re_1 = 391$, respectively. The result that $\langle|\omega^s_{z,tot}|\rangle = 2|a|$ exactly, is a consequence of the boundary condition (22) and is a test of the numerical calculation. Equation (22) implies that the vorticity in the axial direction can only be rearranged by the Taylor instability, its total amount being fixed by the rotation rate of the cylinders.

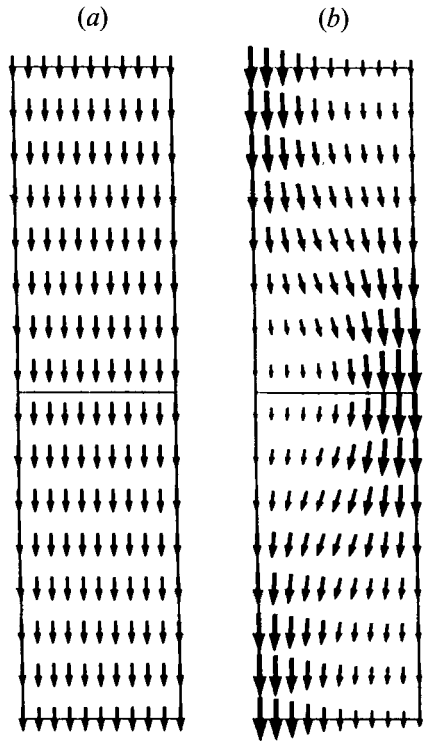

FIGURE 5. Vortex lines direction field in the (r, z)-plane: (*a*) in the Couette state at $Re_{1c} = 371$; (*b*) in the Taylor–Couette state at $Re_1 = 391$.

We now relate our computed results to the observations. Swanson & Donnelly (1991) measured the attenuation α_ϕ which second sound, travelling in the azimuthal direction, suffers owing to the presence of quantized vorticity. At very small Reynolds number, they found $\alpha_\phi = 0$, thus confirming the existence of a vortex-free state already observed in the case of equilibrium flow in a rotating annulus (Bendt 1967). This vortex-free state extends up to the Reynolds number Re_1^* at which vortices appear in the system. Theoretical predictions of Re_1^* in this non-equilibrium flow are not in complete agreement with the recent observations (Swanson 1992; Swanson & Donnelly 1987), but this issue does not concern us here because we can apply the HVBK model only at Reynolds numbers larger than Re_1^*. At $Re_1 > Re_1^*$, Swanson & Donnelly observed that the attenuation is linearly proportional to Re_1. This is consistent with our assumption that the superfluid is in the Couette state with uniform vorticity because $2|a|$ is proportional to Re_1. If Re_1 is further increased, eventually a critical value Re_{1c} is found at which the curve α_ϕ *vs.* Re_1 exhibits a break. This measured value of Re_{1c} is in agreement with our prediction that Couette flow becomes unstable (Barenghi & Jones 1988; Barenghi 1992). At values of Reynolds number higher than Re_{1c} helium is in Taylor flow. Swanson & Donnelly determined that the second sound attenuation is still linearly proportional to Re_1, but the slope is higher than at values of Reynolds number below the break at Re_{1c}. To understand this observation and to relate the results of our calculation to the measurements, we need a model of how second sound interacts with the vortex lines. Let us consider a simple configuration in which the superfluid has constant vorticity $2\boldsymbol{\Omega}$ due to rotation at angular speed Ω in the direction $\hat{\boldsymbol{\Omega}} = (m_1, m_2, m_3)$ where m_1, m_2 and m_3 are directional cosines. Neglecting viscous

dissipation, the wave equation is obtained by linearizing the HVBK equations together with the laws of conservation of mass and entropy; one finds

$$\frac{\mathrm{d}^2\boldsymbol{q}}{\mathrm{d}t^2} = (B'-2)\,\boldsymbol{\Omega}\times\frac{\mathrm{d}\boldsymbol{q}}{\mathrm{d}t} + c_2^2\,\boldsymbol{\nabla}(\boldsymbol{\nabla}\cdot\boldsymbol{q}) + B\hat{\boldsymbol{\Omega}}\times\left(\boldsymbol{\Omega}\times\frac{\mathrm{d}\boldsymbol{q}}{\mathrm{d}t}\right), \tag{25}$$

where $\boldsymbol{q} = \boldsymbol{v}^n - \boldsymbol{v}^s$ and c_2 is the second sound speed. Equation (25) shows that the attenuation is determined by the first mutual friction coefficient B; the second coefficient B' is only a correction to the Coriolis force and modifies the coupling of transverse modes already introduced by the rotation. Let us suppose that the wave has frequency σ and propagates in the x-direction with dependence $\exp(\mathrm{i}\sigma t - \mathrm{i}kx)$. The quantity Ω_1/σ is usually very small. For example, at the temperature $T = 2.1$ K, using the dimensions of Swanson & Donnelly's apparatus (gap width $\delta = 0.0474$ cm, height of the cylinders $h = 9.436$ cm), at Reynolds number $Re_1 = 391$ we find that $\Omega/\sigma = 0.10\times10^{-3}$ and 0.51×10^{-4} for the fundamental axial and radial mode, respectively. At first order in Ω_1/σ, it follows from (25) that $k = \sigma/c_2 - \mathrm{i}\alpha_1$ where α_1 is the attenuation coefficient in the x-direction:

$$\alpha_1 = B\Omega(m_2^2+m_3^2)/2c_2. \tag{26}$$

Note the dependence of the attenuation in the direction 1 on the directional cosines of directions 2 and 3. For example if the vortices are transverse to the direction of sound and $m_2 = 1$, $m_3 = 0$, then the attenuation $\alpha_1 = B\Omega/2c_2$ is maximum; if they make an angle θ with this direction then $m_2 = \sin\theta$, $m_3 = 0$ and $\alpha_1 = B\Omega\sin^2\theta/2c_2$. This last dependence of the attenuation on θ has been verified experimentally (Swanson & Donnelly 1987).

Now equation (26) for the attenuation was derived on the assumption that the vorticity is a constant vector $\boldsymbol{\omega}$. To make use of (26) in our problem we assume that the components of this vector $\boldsymbol{\omega}$ have values $\omega_r = \langle|\omega^s_{r,tot}|\rangle = 44.6$, $\omega_\phi = \langle|\omega^s_{\phi,tot}|\rangle = 5.0$, and $\omega_z = \langle|\omega^s_{z,tot}|\rangle = 386.25$. Note that we use the absolute values of the vorticity because second sound cannot discriminate the sense in which the vortex lines point. The attenuation in the azimuthal direction is then proportional to $|\boldsymbol{\omega}|(m_2^2+m_3^2) = (\omega_r^2+\omega_z^2)/|\boldsymbol{\omega}|$. We have seen already that, owing to the boundary condition $v^s_\phi = 0$, the average axial vorticity in Taylor flow is the same as in Couette flow: $\omega_z = 2|a|$. Since the transition to Taylor cells is a pitchfork bifurcation, we expect that the amplitude of the nonlinear solution to be proportional to $(Re_1 - Re_{1c})^{\frac{1}{2}}$ close to the critical Reynolds number. Hence both ω_r^2 and ω_ϕ^2 will be proportional to $(Re_1 - Re_{1c})$ near critical, so

$$\alpha_\phi \cong 2|a|\,(1+K(Re_1 - Re_{1c})), \tag{27}$$

where K is some constant. Equation (27) explains why the second sound attenuation is linearly proportional to Re_1 even in the Taylor flow regime, as observed by Swanson & Donnelly.

We now compare the observed values of the attenuation with the experiment. From the previous discussions, we have that the attenuations of second sound travelling in the azimuthal, radial and axial directions are respectively

$$\alpha_r = \frac{B}{2c_2}\frac{\omega_\phi^2+\omega_z^2}{|\boldsymbol{\omega}|} = 386.2, \quad \alpha_\phi = \frac{B}{2c_2}\frac{\omega_r^2+\omega_z^2}{|\boldsymbol{\omega}|} = 391.3,$$

$$\alpha_z = \frac{B}{2c_2}\frac{\omega_r^2+\omega_\phi^2}{|\boldsymbol{\omega}|} = 5.2 \quad \text{where} \quad |\boldsymbol{\omega}| = 386.3.$$

In the Couette flow state at the critical Reynolds number the attenuations are

respectively $\alpha_r^\circ = 2|a^\circ| = 366.5$, $\alpha_\phi^\circ = 2|a^\circ| = 366.5$ and $\alpha_z^\circ = 0$. Thus α_z suffers the largest relative change in the transition from Couette to Taylor flow. This is consistent with Swanson & Donnelly's report (1991) that the percentage change in attenuation is greater for the axial resonance mode than for the azimuthal one.

Swanson & Donnelly also present a graph of $\xi = A/A_0 - 1$ *vs.* Re at $T = 2.1$ K, where A and A_0 are the amplitudes of the resonances of a second sound azimuthal mode measured with and without vortices. Thus ξ is proportional to the attenuation coefficient α_ϕ. The graph shows a break of the slope of ξ *vs.* Re_1 around $Re_{1c} = 336$, which corresponds to the onset of toroidal motion; at this point we read $\xi^0 = \xi^0(Re_1 = 336) = 0.25$. We can also read that 5.4% above onset $\xi(Re_1 = 354) = 0.28$, so the relative change is small: $(\xi - \xi^0)/\xi^0 = 12\%$ only. This value should be compared with the relative change $(\alpha_\phi - \alpha_\phi^0)/\alpha_\phi^0 = 6.8\%$ which results from our calculation at Reynolds numbers 371 and 391 at $T = 2.1$ K of figures 1–5. We conclude that our nonlinear calculation of the attenuation is in order-of-magnitude agreement with the experiment. The value $\xi = 0.28$ is probably an upper bound since it is obtained from the line which fits the data at high values of Re_1 and there is usually some rounding of the attenuation near the onset. In addition the attenuation measured will depend on the detailed spatial structure of the mode used to probe the flow. Figure 5(*b*) shows the direction of the vortex lines in the (r, z)-plane at $Re_1 = 391$. It can be seen that the vorticity in the z-direction is higher near the walls whilst the vorticity in the r-direction is higher in the centre of the cells.

5. Conclusions

We conclude that for the first time we have solved the nonlinear HVBK equations and determined the finite-amplitude solution above the critical velocity at which Couette flow becomes unstable. We find that in our axisymmetric flow satisfactory results are obtained when the boundary conditions on the superfluid at the cylinders are taken as $\omega_\phi^s = v_\phi^s = 0$, which implies that the superfluid vorticity and velocity are both purely axial there.

These investigations have so far only treated the mildly supercritical regime and here we have found that the quantized vortex lines are still predominantly aligned along the axis of rotation as in the Couette state, and that the deflection in the azimuthal direction is smaller than radial deflection. The pattern of the normal fluid flow is broadly similar to that found in classical Taylor–Couette flow, but the pattern of the superfluid flow is markedly different; instead of a meridional flow consisting of a single pair of cells in each period, we find a more complex pattern of eddies and counter-eddies.

The results have been interpreted in terms of the effects on the attenuation of second sound propagating in the three orthogonal directions. Comparison with the existing measurements shows there is order of magnitude agreement between the theoretical and experimentally observed change in azimuthal second sound attenuation. However, a more detailed analysis of the attenuation found in the experiments will be necessary before detailed quantitative agreement can be found.

This research is supported by SERC grant number *GR/H*38003.

REFERENCES

AARTS, R. G. K. M. & WAELE, A. T. A. M. DE 1994 *Physica* B **194–196**, 725.

ANDRONIKASHVILI, E. L. & MAMALADZE, YU. G. 1966 *Rev. Mod. Phys.* **38**, 567.

BARENGHI, C. F. 1991 *J. Comput. Phys.* **95**, 175.

BARENGHI, C. F. 1992 *Phys. Rev.* B **45**, 2290.

BARENGHI, C. F., DONNELLY, R. J. & VINEN, W. F. 1993 *J. Low Temp. Phys.* **52**, 189.

BARENGHI, C. F. & JONES, C. A. 1988 *J. Fluid Mech.* **197**, 551.

BARENGHI, C. F., SWANSON, C. J. & DONNELLY, R. J. 1994 *J. Low Temp. Phys.* (to appear).

BEKHAREVICH, I. L. & KHALATNIKOV, I. M. 1961 *Sov. Phys. J. Exp. Theor. Phys.* **13**, 643.

BENDT, P. J. 1967 *Phys. Rev.* **153**, 280.

BIELERT, F. 1993 PhD. thesis, University of Göttingen.

CAMPBELL, L. J. & ZIFF, R. M. 1978 *Phys. Rev.* B **20**, 1886.

CHANDRASEKHAR, S. 1961 *Hydrodynamics and Hydromagnetic Stability*. Oxford University Press.

CHANDRASEKHAR, S. & DONNELLY, R. J. 1957 *Proc. R. Soc. Lond.* A **241**, 9.

DI PRIMA, R. C. & SWINNEY, H. L. 1981 In *Hydrodynamic Instabilities and Transition to Turbulence* (ed. H. I. Swinney & P. Gollub), p. 139. Springer.

DONNELLY, R. J. 1991 *Quantized Vortices in Helium II*, Cambridge University Press.

DONNELLY, R. J. & LAMAR, M. M. 1988 *J. Fluid Mech.* **186**, 163.

DONNELLY, R. J. & SWANSON, C. E. 1986 *J. Fluid Mech.* **173**, 387.

HALL, H. E. 1960 *Phil. Mag. Suppl.* **9**, 89.

HALL, H. E. & VINEN, W. F. 1956*a* *Proc. R. Soc. Lond.* A **238**, 204.

HALL, H. E. & VINEN, W. F. 1956*b* *Proc. R. Soc. Lond.* A **238**, 215.

HILLS, R. N. & ROBERTS, P. H. 1977 *Arch. Rat. Mech. Anal.* **66**, 43.

JONES, C. A. 1985 *J. Comput. Phys.* **61**, 321.

KHALATNIKOV, I. M. 1965 *An Introduction to the Theory Superfluidity*. Benjamin.

MATHIEU, P., PLACAIS, B. & SIMON, Y. 1984 *Phys. Rev.* B **29**, 2489.

NORTHBY, J. A. & DONNELLY, R. J. 1970 *Phys. Rev. Lett.* **25**, 214.

SCHWARZ, K. W. 1988 *Phys. Rev.* B **38**, 2398.

SNYDER, H. A. 1974 *Proc. 13th Intl Conf. Low Temp. Phys. LT13*, **1**, 283. Plenum.

SWANSON, C. J. 1992 Appearance of vortices and stability of the Taylor–Couette flow of helium II. PhD thesis, University of Oregon.

SWANSON, C. E. & DONNELLY, R. J. 1987 *J. Low Temp. Phys.* **67**, 185.

SWANSON, C. J. & DONNELLY, R. J. 1991 *Phys. Rev. Lett.* **67**, 1578.

TOUGH, J. T. 1982 *Progress of Low Temperature Physics*, vol. 8 (ed. D. F. Brewer). North Holland.